# SIMULATION OF ORBITAL RADAR IMAGES

R. S. Saunders

Jet Propulsion Laboratory
California Institute of Technology
Pasadena, California 91103

J. C. Holtzman

University of Kansas
Lawrence, Kansas 66044

Charles Elachi

Jet Propulsion Laboratory
California Institute of Technology
Pasadena, California 91103

ABSTRACT

Many of the questions that arise concerning the operating parameters for spaceborne synthetic aperture imaging radar systems can be addressed in a cost-effective manner by using simulation techniques. This can include use of airborne images, Seasat images, and computer simulation. The first computer simulation of spaceborne radar imagery has been analyzed for system definition studies. Analysis of the simulation indicates that incidence angles as small as 30° are useful for general terrain geomorphologic analysis.

## I. INTRODUCTION

The Seasat imaging experiment has demonstrated the feasibility of an orbiting synthetic aperture imaging radar system. The land images contain a wide variety of geologic features (Figure 1) and preliminary analyses indicate that the Seasat images may be a useful geologic mapping tool in certain types of terrain (Elachi, 1980; Ford, 1980; Stewart, 1980) where the relief is low to moderate.

Previous studies have indicated that, for airborne systems, the optimum incidence angle (Figure 2) depends on the terrain (MacDonald and Waite, 1971). Similarly, with stereo, the pair of incidence angles that yields the strongest visual stereo model may depend on the terrain. Opposite side stereo at 45° incidence provides the largest vertical exaggeration, but may only be usable

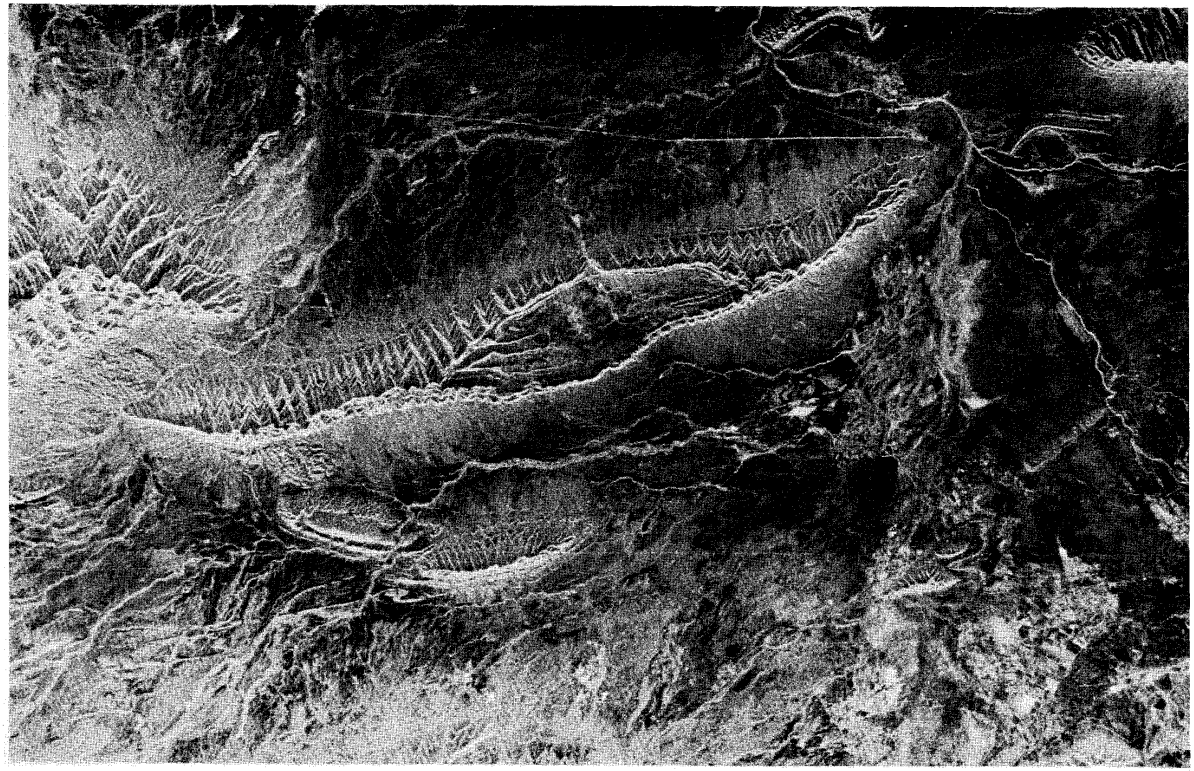

Figure 1. Breached doubly-plunging anticlines in Cretaceous sedimentary rocks west of Obayos, Coah., Mexico, as seen by Seasat imaging radar. The axes of two of the anticlines are oriented near-normal to the radar look-direction (approximately N 70° E). The layered character of the rocks is denoted by flatiron patterns on the northeast-facing flanks of the anticlines. Compression of the southwest-facing flanks is caused by foreshortening due to radar layover.

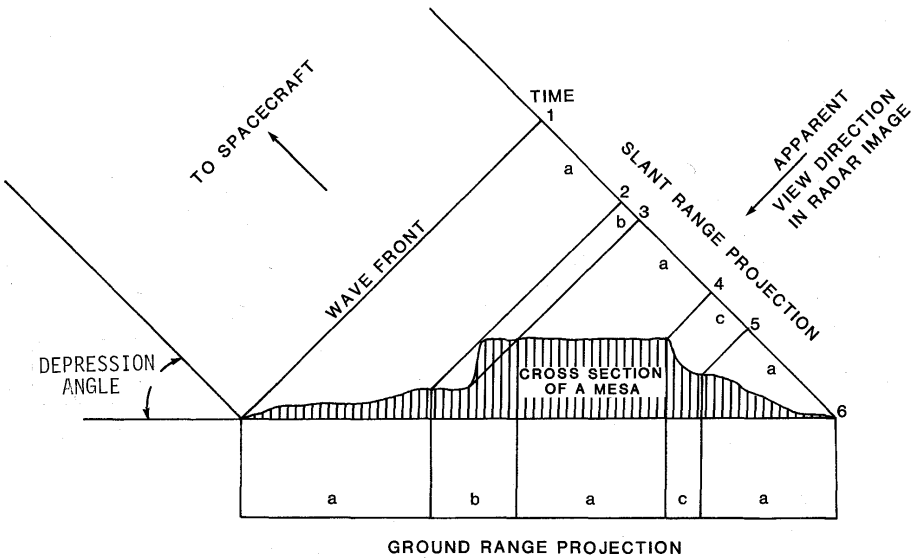


Figure 2. Illustration of layover and shadow. For spaceborne geometry note that there is little change in incidence angle across the scene. The wave front strikes the surface and is reflected back and its intensity recorded as a function of time. Between time 1 and 2, normal image is obtained (a). Between time 2 and 3, the plateau top and the area near the cliff base are at the same range and thus overlap in the image, a condition known as layover (b). No reflection is recorded between time 4 and 5, resulting in radar shadow (c).

in areas of relatively flat terrain. Other pairs may be most useful in mountainous regions.

Three current imaging radar experiments have faced the necessity of defining operating parameters for a spaceborne SAR. These are the Seasat SAR experiment, the Shuttle Imaging Radar (SIR-A) and the Venus Orbiting Imaging Radar (VOIR) SAR Experiment.

The Seasat SAR was designed to image the ocean surface rather than the land, and no consideration was given to the problem of layover (Figure 2) in the land images where the local slopes exceed the incidence angle. Nevertheless Seasat images are useful for studies of land use and structural analysis in moderate to low relief regions (Bryan, 1980; Sabins et al., 1980).

SIR-A was specifically designed to assess the utility of imaging radar as an aid to geologic mapping. It has been generally assumed that the optimum incidence angle for this purpose must be large, certainly large enough to avoid layover, and preferably large enough to provide shadow. This perception apparently arises from experience with airborne SAR images. The only such images available were obtained by systems developed for the military. Although the images taken with extreme (60° - 80°) incidence angle superficially resemble air photos in their maplike appearance and shading, a primary consideration in the design of these systems appears to be a desire to avoid flying close to the enemy positions. Very little high quality radar imagery is available at low incidence angles for comparative studies. The SIR-A team grappled with the question of incidence angle and decided on about 50° as a good compromise for the widest variety of geologic terranes.

The VOIR Science Working Group faced the same problems. In general such problems as wavelength selection, resolution requirements and radiometeric quality of the image, although by no means trivial, can be addressed with existing experience. The question of incidence angle for Venus could not be as easily decided. At one extreme, it may be argued that Venus is dominated by modest slopes as seen in the existing Earth-based radar images (Figure 3) and the Pioneer Venus altimetry. The argument is that very low incidence angles provide resolution of small slope changes because of the steepness of the backscatter function in that region (Figure 4). At the other extreme is terrestrial experience suggesting that shadow may be essential to geomorphological analysis, and that high (>60°) incidence angles are needed. Meanwhile, the radar system analysis demonstrates that high incidence angles for orbital systems can only be obtained with very large (and expensive) antennas and from a practical standpoint the incidence angle cannot exceed 50° by a significant amount. For VOIR a 50° incidence angle was requested by the science investigators and remains the baseline design. From the above, it is clear that uncertainties about the viewing geometry that is best for imaging various terrains dominate the design concerns. Since we have no practical way of obtaining orbital images with varying incidence angles, other approaches have been devised to study this parameter. These involve simulations using airborne and computer-generated images.

In general, airborne images have considerable variation in incidence angle across the swath. To produce images with less variation, multiple close tracks were flown over a region of northern Arizona so that a mosaic could be assembled from small strips with 5° or less variation of incidence angle across them.

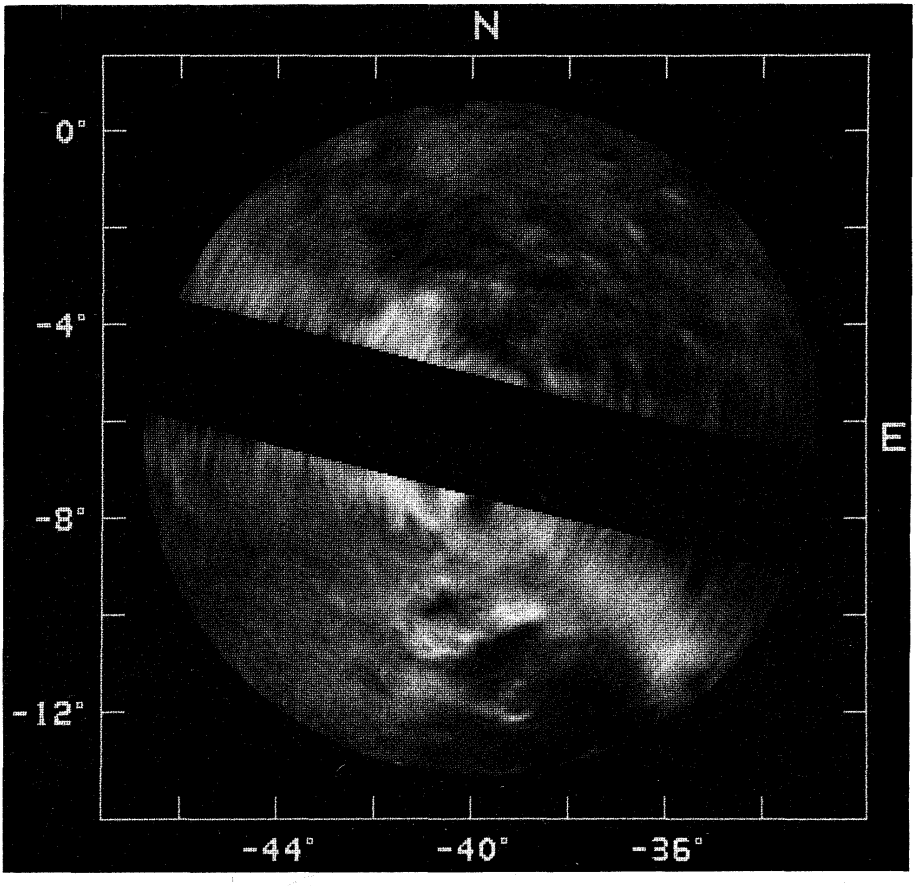


Figure 3. Earth-based radar image of a portion of Venus approximately 1500 km across. The dark band is a region that cannot be unambiguously imaged. This image shows that at incidence angles of 4° to 6° a very small change in slope can be detected. The circular craterlike feature in the lower half has slopes of less than one degree. Image courtesy Raymond Jurgens, JPL.

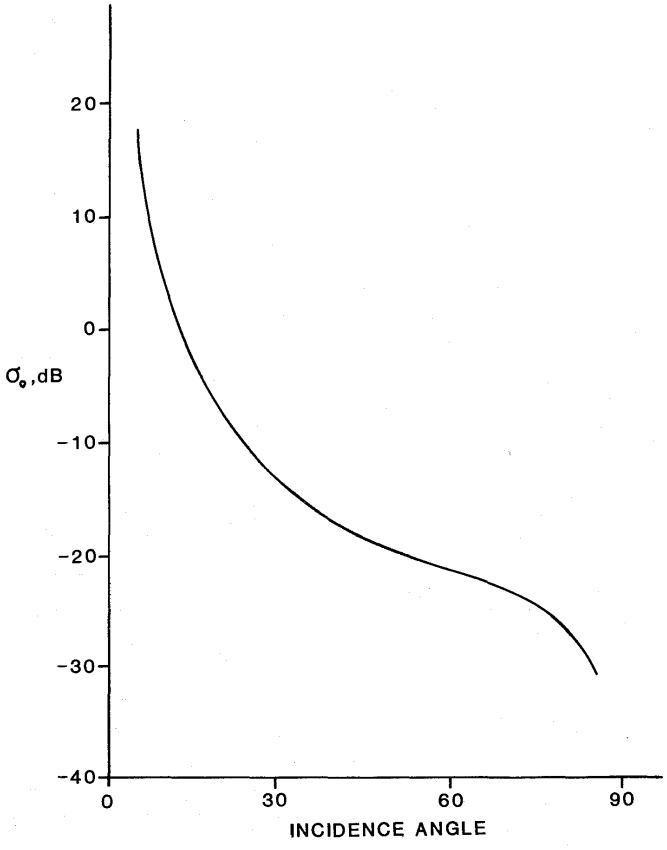


Figure 4. Typical backscatter function for a dry cinder surface of L-band, like-polarized. Note that near zero incidence, the backscatter is most sensitive to small changes in slope.

The other approach is to use computer image simulation to study the effects of varying the incidence angle. In this approach we used the "Point Scattering Model" developed at the University of Kansas (Holtzman et al., 1978).

## II. SIMULATION OF ORBITAL GEOMETRY USING AIRBORNE IMAGES

The JPL L-band airborne SAR system was used to simulate orbital geometry. Conventional airborne SAR images typically have a range of incidence angle of more than 10°. For the simulation, a region of northern Arizona that includes part of the Grand Canyon and the San Francisco Mountains was chosen. The flight paths for the image strips were chosen to provide closely overlapping images from several directions. The system can operate in two modes, one that images from nadir (0° incidence) out to 45° and a second that images the area from 40° out to about 60°. An example of the imagery from nadir to 45° is shown in Figure 5. These images were cut into strips having a narrow ($\leq$ 5°) band of incidence angle and mosaicked to produce images having incidence angles near 45° and 55° (Figure 6).

## III. COMPUTER SIMULATION

Techniques for computer simulation have been developed at the University of Kansas (Holtzman et al., 1978). Applications to date have been in simulation of airborne images. Here we present the first results of computer simulation of spaceborne radar images.

Radar images have been successfully generated by digital computers for geoscience and guidance applications using techniques called the Point Scattering Model (PSM). The PSM provides the flexibility required to efficiently simulate, by digital means, the radar image products of a wide variety of radar systems for diverse target scenes.

The PSM is centered around a closed-system description of the microwave imaging process. This description rigorously treats the closed-system consisting of the radar transmitter and receiver, the ground dielectric properties, the geometric orientation of target features, and the data recording medium. The random nature of this system is also modeled. The process of simulating radar images via the PSM includes acquiring input data about the ground scene, radar system, and vehicular position. Also, an imaging process transfer function must be implemented which implies recognition of resolution cell boundaries. Succeeding algorithms must then relate the backscattered or reflected microwave signals to the synthesized image.

Important in the simulation of radar imagery is establishment of an accurate "ground model" which will be relevant for microwave remote sensors. By appeal to the classical radar equation relating the average radar return power to the transmitted power, and to the target cross section ($\sigma$). Alternately, we may model the ground by $\sigma^o$ and elevation samples, from which slope information can be derived. These data go into the making, but are not synonymous with the "ground truth data base" (hereafter referred to as data bases) upon which the implementation algorithms operate.

The data base can be in the form of a rectangular matrix (facilitating digital implementation). It represents the sampled version of the ground scene by storing (1) backscatter category (e.g., pasture) and (2) elevation. The distinction between the ground model and the data base is seen to be the use of

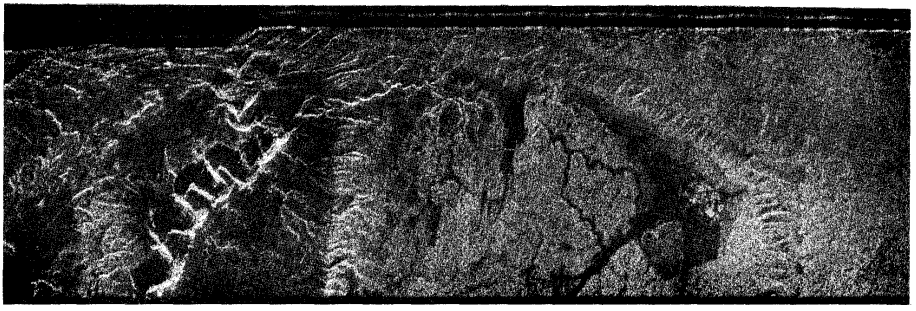

Figure 5. JPL L-band image of nadir out to 45°. Many such strips were used to produce the mosaics of Figure 7. The top of the image is the nadir and is essentially a profile of land surface beneath the aircraft ground track.

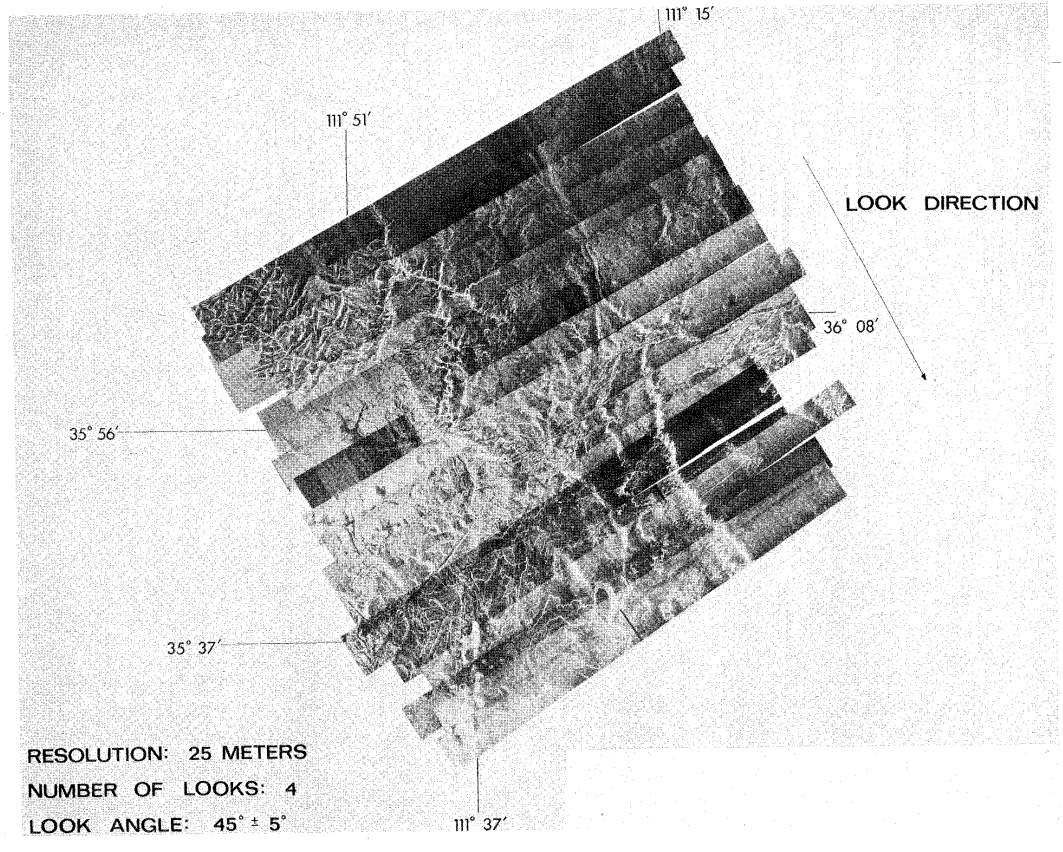


Figure 6. Airborne radar image mosaics obtained at two different look angles, 45° and 55°. The mosaic covers the San Francisco volcanic field and the southern rim of the Grand Canyon.

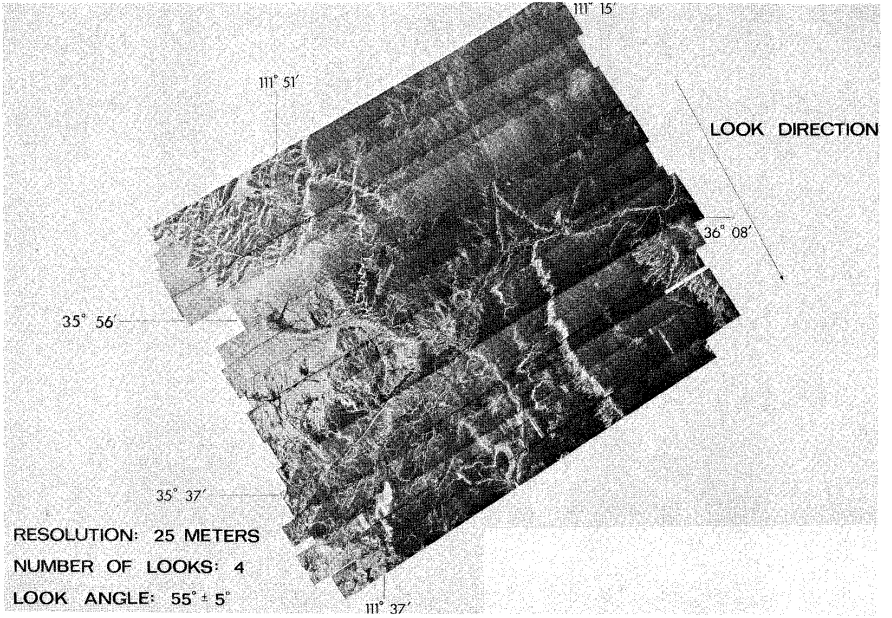


Figure 6 (contd)

category rather than $\sigma^o$ in the data base. This is done because $\sigma^o$ is a function not only of the backscattered category, but also the radar incidence angle with respect to the resolution cell, frequency, polarization, etc. Therefore, storing $\sigma^o$ in the data base would limit the data base utility to simulations with a fixed radar look direction and incidence angle, etc.

Data bases have been constructed from two sets of source data: available digital elevation tapes and geometrically rectified aerial photography. The purpose of the imagery (which is not suggested to be limited to air photos; infrared and radar imagery can be instrumental) is to allow a photo/radar-interpreter to delineate boundaries of distinct backscatter regions. The interpreter produces an outline map for the target scene, separating different radar scattering (or reflecting) objects. This line drawing is digitized, and the digitized "category" data are oriented properly into a rectangular matrix to be merged with the elevation data matrix.

The next step is to calculate the return power from each of the resolution cell areas. For medium resolution radar systems, these areas can be simulated independently. The simplification allowed by ignoring the effect of adjacent cells greatly reduces the computational complexity of the problem. The information of adjacent cells is needed only to calculate the slopes of each cell and to calculate the effects of radar "shadow," "layover," and "fore-shortening." At each cell the local incidence angle is calculated from the radar incidence angle and the local terrain slope at the cell. The category information stored at each cell describes the backscatter target type represented by the area. By use of a curve, fit to empirical or theoretical backscatter data for the category, a $\sigma^o$ value for the specific angle of incidence is determined. This information is used to calculate the return power from each resolution cell area by application of the general radar simulation model.

The final step is to produce an output image. The array of return powers calculated in the previous step is converted to relative greytones representing density on photographic film. Each greytone value represents the return from a specific resolution cell area on the ground. The final image product is displayed and then photographed.

This summary of the Point Scattering Model and associated techniques has been presented in order to explain how radar image simulations (for distributed targets) are generated. Simulation results have been compared against actual radar imagery of the test terrain sites, with positive results. For example, Figure 7 illustrated real radar and simulated radar imagery.

For the VOIR space simulation we used the topographic file produced by the Defense Mapping Agency of the Flagstaff (NI 12-2) Quadrangle. The resolution of the data set is 200 feet with 50 foot contour intervals (Figure 8). In the simulation we have an east look direction from an altitude of 300 km. The incidence angles chosen are 23°, 30°, 50°, and 70°. A single class of terrain was used for the entire image: dry soil with a roughness of 2.0 cm RMS height and moisture content of .03 $g/cm^3$. The simulation has a resolution of 61 m along track and 76 m across track at 50° (Figure 9).

The results of the simulation suggest that for this area, an incidence angle of 30° provides full interpretability. Less than 30° introduces layover which complicates the interpretation but greater than about 50° appears in this

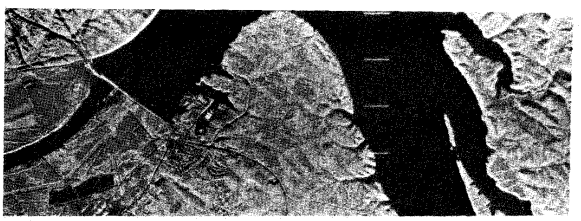

APD-10 SAR IMAGE Resolution 10 Feet

3.23 miles

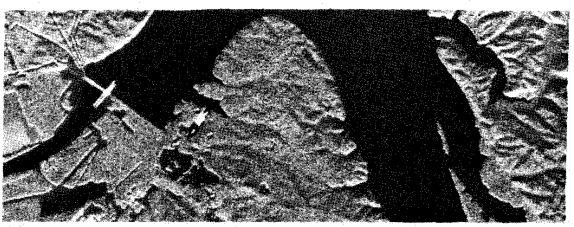

SIMULATED RADAR IMAGE Resolution 60 Feet

3.23 miles

Radar Look-Direction

Figure 7. Simulated radar image compared to SAR image of Pickwick Dam site.

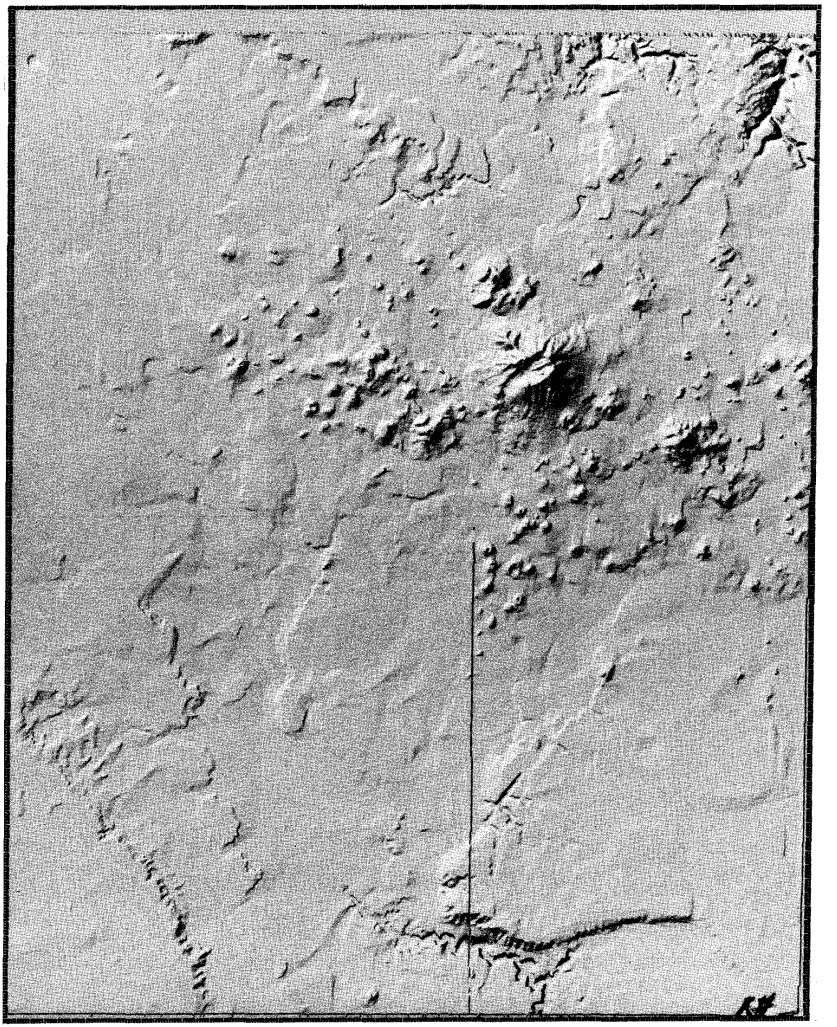

Figure 8. Shaded relief version of the DMA digital topographic data base used in the computer simulations. Image processing was done at the JPL Image Processing Laboratory.

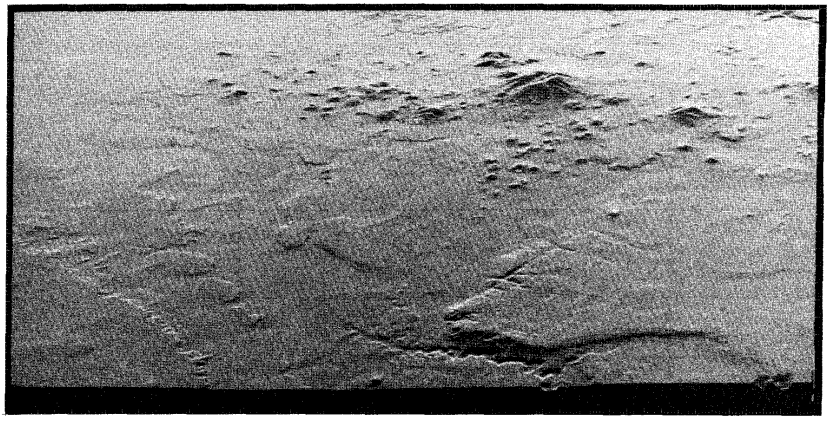

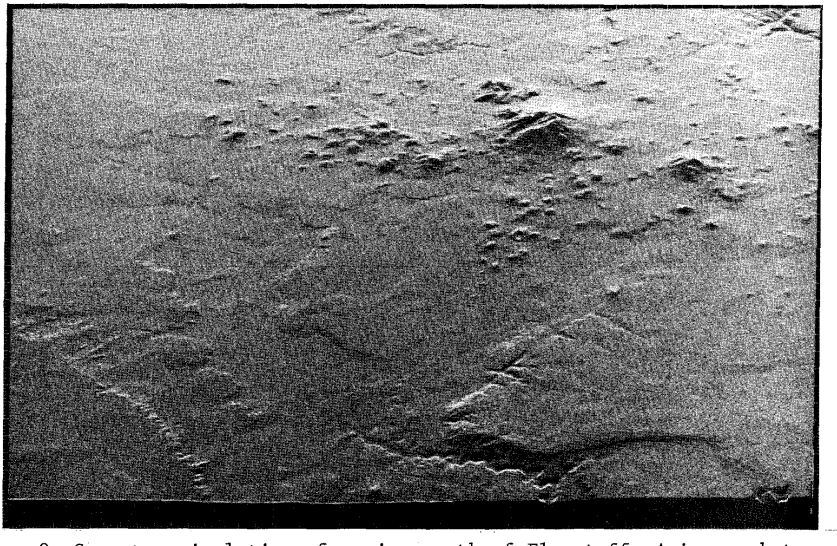

Figure 9. Computer simulation of region north of Flagstaff, Arizona, between the San Francisco Peaks and the Grand Canyon. The simulation illustrates the effect of varying incidence angle. The resolution in each case is 200 feet (60 meters). In all views, south is at the top. (a) through (d) are in slant range projection. Incidence angle is (a, top) 23° (b, bottom) 30° (c, page 59) 50° (d, page 60) 70°. In 9 (e, page 61) the 30° incidence simulation is presented in a ground range projection. Figure 9 (f, page 62) shows the same region in a digitally processed JPL Seasat image which was imaged from a different direction. The digital simulations were done at the Remote Sensing Laboratory of the University of Kansas Center for Research, Inc. Digital to film processing, enhancement, and geometric transformations were done at the JPL Image Processing Laboratory.

Figure 9 (contd)

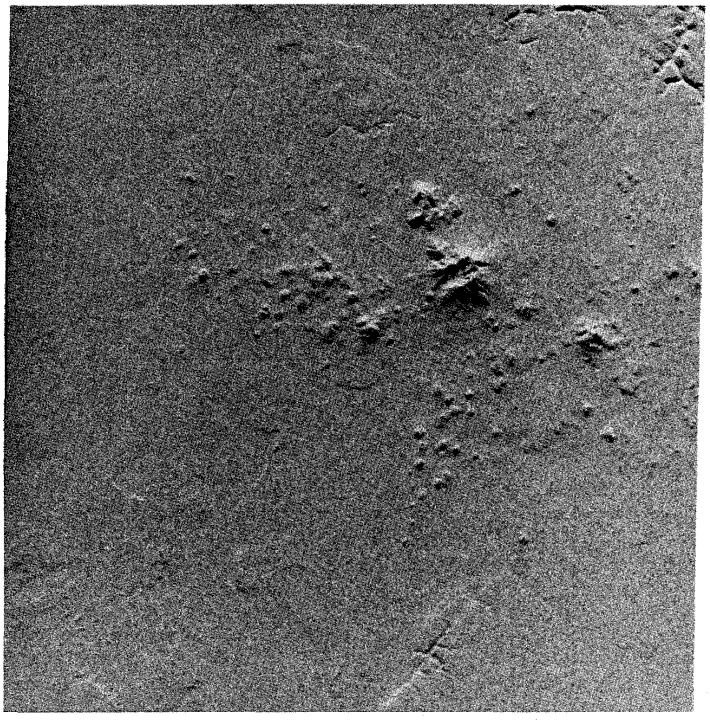

Figure 9 (contd)

Figure 9 (contd)

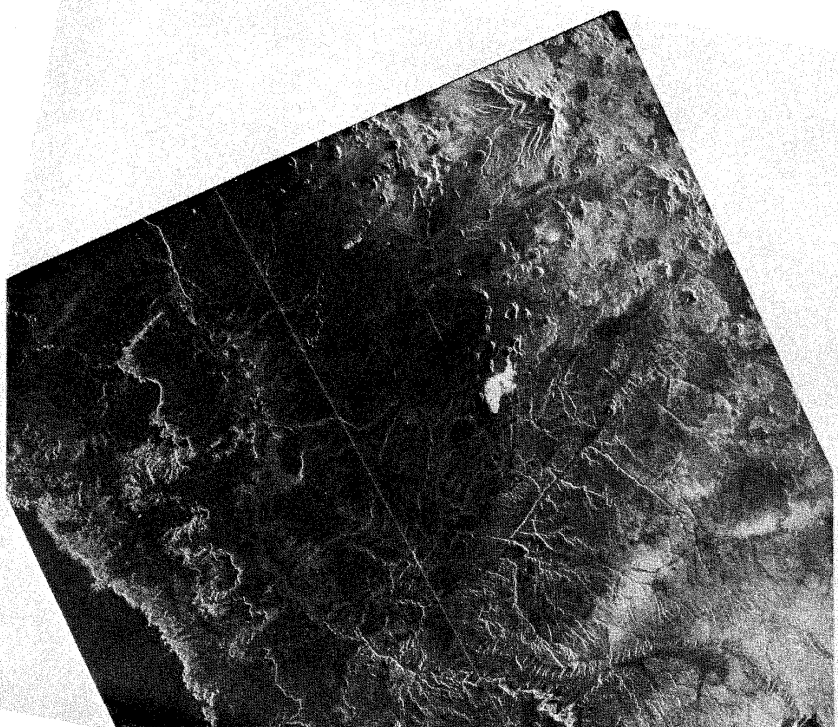

Figure 9 (contd)

simulation to actually degrade the interpretability. Further simulations in other terrains must be performed to assess the significance of these observations.

## REFERENCES


Bryan, M. L., Radar Study of Vegetated Pediment (submitted to Science).

Elachi, C., Spaceborne Imaging Radar in Oceanography and Geology, Science, 205, (in press), 1980.

Ford, J. P., Analysis of Seasat Orbital Radar Imagery for Geologic Mapping in the Appalachian Valley and Ridge Province, Tennessee - Kentucky - Virginia: This Volume.

Holtzman, J. C., Frost, V. S., Abbott, J. L., and Kaupp, V. H., "Radar Image Simulation," IEEE Trans. on Geoscience Electronics, Vol. GE-16, No. 4, Oct. 1978.

MacDonald, H. and Waite, W., Optimum Radar Depression Angles for Geological Analysis: Modern Geology, 2, 179-193, 1971.

Sabins, F. F., Blom, R., and Elachi, C., Expression of San Andreas Fault on Seasat Radar Image: Bull. AAPG, 64, (in press), 1980.

Stewart, H. E., Blom, R., Abrams, M., and Daily, M., Rock Type Discrimination and Structural Analysis with Landsat and Seasat Data: San Rafael Swell, Utah: This Volume.